Organic Microlasers

DOI: 10.1002/anie.201310659

Whispering-Gallery-Mode Microlaser Based on Self-Assembled Organic Single-Crystalline Hexagonal Microdisks**

Xuedong Wang, Qing Liao, Qinghua Kong, Yi Zhang, Zhenzhen Xu, Xiaomei Lu, and Hongbing Fu**

Abstract: *Whispering-gallery-mode (WGM) resonators of semiconductor microdisks have been applied for achieving low-threshold and narrow-linewidth microlasers, but require sophisticated top-down processing technology. Organic single-crystalline hexagonal microdisks (HMDs) of p-distyrylbenzene (DSB) self-assembled from solution can function as WGM microresonators with a cavity quality factor (Q) of 210. Both multiple- and single-mode lasing had been achieved using DSB HMDs with an edge length of 4.3 and 1.2 μm, respectively. These organic microdisks fabricated by bottom-up self-assembly approach may offer potential applications as low-threshold microlaser sources for photonic circuit integration.*

Semiconductor microdisks have attracted a great deal of interests for the development of microlasers,[1] and for the fundamental investigation of light–matter interactions.[2] Because of the large refractive index contrast between semiconductor material and its surrounding, photons are strongly confined within microdisk whispering-gallery-mode (WGM) resonator by means of successive total internal reflection along the disk circumference. Therefore, semiconductor microdisk WGM microresonator features low optical loss (i.e., high Q) and small mode volume (V) for integration of miniaturized devices.[3,4] For example, Tamboli et al. report room-temperature continuous-wave lasing in GaN/InGaN microdisks.[5] Recently, Chen et al. demonstrated that tapered InGaAs/GaAs core/shell nanopillar lasers grown on silicon substrate can support WGM-like helically propagating mode with a measured Q of 319 and a lasing threshold of 93 μJ cm^{-2}.[6] Nonetheless, most of the semiconductor microdisks have been fabricated through top-down method,[7] which requires numerous fabrication steps as well as subsequent patterning techniques. Most recently, it had been demonstrated that bottom-up synthesized microstructures, such as ZnO microdisks, exhibited many advantages over top-down fabricated devices, including smooth outer surfaces, high crystallinity, and high-throughput assembly.[4,8]

As compared with their inorganic counterparts, organic semiconductors have several inherent advantages, such as amenability to low-cost and low-temperature processing, and compatibility with plastic substrates.[9] Organic materials had been applied in WGM lasing devices by coating organic polymer on pre-prepared microfiber structures,[10] or by doping organic dyes in spheres.[11] In these laser devices, organic materials are mostly in the form of amorphous or polycrystalline state, which leads to low gain density and large defect density. Therefore, these laser devices were usually large, and exhibited a relatively high lasing-threshold.

Recently, self-assembled and well-faceted single-crystalline one-dimensional (1D) nanowires of organic semiconductors have been demonstrated as Fabry–Pérot (FP) resonator with two of the optically flat end-faces as two reflectors. Active optical waveguides and optically pumped lasers have been observed because of strong optical confinement in organic nanowires.[12] Herein we reported for the first time WGM microlasers based on self-assembled single-crystalline organic hexagonal microdisks (HMDs) of *p*-distyrylbenzene (DSB) with the edge length (d) ranging from 1.0 to 5.0 μm. Photoluminescence (PL) microscopy reveals alternative bright/dark edges on DSB HMDs as a characteristic of the D3-WGM resonator. Lasing behaviors were observed for DSB HMDs with different edge lengths. And importantly single mode lasing is achieved in a HMD with an edge length of 1.2 μm and a threshold pump density as low as 790 nJ cm^{-2}.

HMDs of DSB were prepared (see the Experimental Section in the Supporting Information) by a facile solution self-assembly method.[13] In a typical synthesis, 20 mg of DSB was completely dissolved in 10 mL of toluene at the boiling point of 110 °C, under refluxing protected by N_2. Then the solution was cooling down slowly to room temperature, and HMDs were obtained. PL microscopy (Figure 1 a) and atomic force microscopy (Figure S1) results reveal that as-prepared HMDs have an edge length (d) of 1.0–5.0 μm and a thickness

[*] X. D. Wang, Q. H. Kong, Y. Zhang, Z. Z. Xu, Prof. H. B. Fu
Beijing National Laboratory for Molecular Sciences (BNLMS)
Institute of chemistry, Chinese Academy of Sciences
Beijing 100190 (P.R. China)
E-mail: hongbing.fu@iccas.ac.cn
X. D. Wang, Q. H. Kong, Y. Zhang, Z. Z. Xu
Graduate University of Chinese Academy of Sciences
Beijing 100049 (P.R. China)
Dr. Q. Liao, X. M. Lu, Prof. H. B. Fu
Beijing Key Laboratory for Optical Materials and
Photonic Devices Department of Chemistry
Capital Normal University, Beijing 100048 (P.R. China)
E-mail: liaoqing@cnu.edu.cn

[**] Thanks Prof. Yanke Che, Prof. Yongzhen Huang, and Dr. Lang Wei for discussion. This work was supported by the National Natural Science Foundation of China (grant numbers 21073200, 21273251, 91333111, 21190034, 21221002), Beijing Municipal Science & Technology Commission (grant number Z131103002813097), project of Construction of Innovative Teams and Teacher Career Development for Universities and Colleges Under Beijing Municipality (IDHT20140512), the National Basic Research Program of China (973) (grant numbers 2011CB808402 2013CB933500), and the Chinese Academy of Sciences.

Supporting information for this article is available on the WWW under http://dx.doi.org/10.1002/anie.201310659.

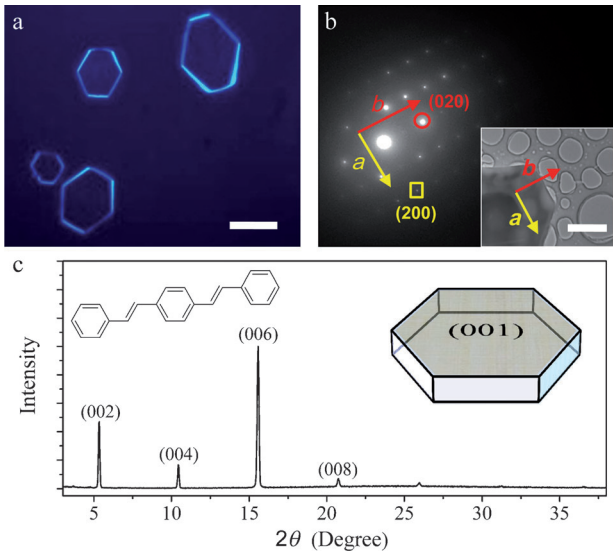

Figure 1. a) Fluorescence microscopy image of the as-prepared HMDs excited with UV band (330–380 nm) from a mercury lamp. b) SAED pattern of one HMD. Inset: the TEM image of the corresponding HMD. c) XRD patterns of HMD assemblies. The left inset: the molecule structure of DSB.

(h) around 350 nm. Figure 1 b depicts the selected area electron diffraction (SAED) pattern, recorded by directing the electron beam perpendicular to the flat surface of a single hexagonal disk. It is known that an orthorhombic crystal of DSB has the lattice parameters of $a = 5.873$ Å, $b = 7.697$ Å, $c = 34.86$ Å, and $\alpha = \beta = \gamma = 90°$. Therefore, the clearly observed SAED spots and its square symmetry suggest that DSB HMDs are single crystals. In Figure 1 b, the squared and circled SAED spots correspond to (200) and (020) crystal planes with d-spacing values of 2.9 and 3.9 Å, respectively. This is also consistent with the X-ray diffraction measurements (Figure 1 c), in which only diffraction peaks correspond to a serial of crystal planes {001}, such as (002), (004), and (006). Combining SAED and XRD results together, we conclude that DSB HMDs adopt a lamellar structure with the crystal (001) plane parallel to the substrate (see inset in Figure 1 c).

DSB molecules adopt a herringbone packing mode in crystals, resulting in H-type aggregates.[14] Because of exciton–vibration coupling effect, the optically forbidden 0–0 transition in H-aggregate system could lead to a reduction of the self-absorption effect and the minimization of direct radiative loss through a 0–0 transition in the typical four-level system of an organic semiconductor laser.[15] Meanwhile the optically allowed 0–n ($n \geq 1$) transitions hold a promise for the strong fluorescence emission with a quantum yield of 65 % of the DSB single crystal.[16] These outstanding optical properties indicate that the DSB material is an excellent candidate for laser action. As shown in Figure 1 a, HMDs exhibit alternative bright/dark edges under excitation of unfocused UV light (330–380 nm). This phenomenon, that is, bright PL spots at the edges and weaker PL from the bodies, indicates that DSB HMDs may serve simultaneously as an optical resonator and an actively gain material.[17]

We further explored the PL properties of an individual DSB HMD using a μ-PL system (Figure S2). The second harmonic ($\lambda = 400$ nm, pulse width 150 fs) of a 1 KHz Ti:sapphire regenerative amplifier is focused to a 20 μm-diameter spot to uniformly excite the isolated single HMD placed on a quartz plate. Figure 2 a shows a typical PL spectrum obtained from a HMD with $d = 3.0$ μm (Figure 2 b). For

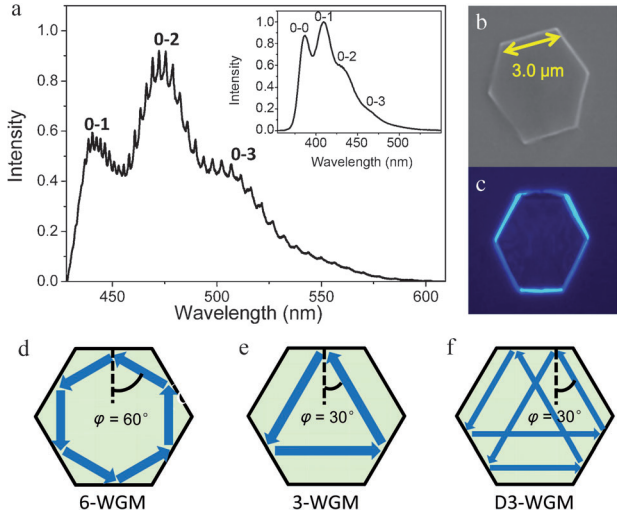

Figure 2. a) μ-PL spectrum (solid line) of a DSB HMD with edge length $d = 3.0$ μm. Inset: PL spectrum of DSB monomers in THF solution. b) The SEM image of this HMD. c) The fluorescence microscopy image of this HMD. d,e,f) Schematic pictures of the light path of the 6-WGMs (d), 3-WGMs (e), and D3-WGM (f). And the angle ϕ denotes the angle of incidence.

comparison, the PL spectrum of DSB monomers in THF solution (inset of Figure 2 a) is also included. The PL spectrum of HMDs exhibits a vibronic progression composed of 0–1, 0–2, and 0–3 bands at 440, 475, and 510 nm, respectively, with a sub-band spacing of 1400 cm^{-1} arising mainly from vinyl stretching modes,[18] while the 0–0 emission is absent because of its optically forbidden nature in highly ordered H-aggregates of single-crystalline DSB HMDs. Notably, as compared with the smooth profile of the monomer PL spectrum (inset in Figure 2 a), a series of sharp peaks are observed on the top of 0–1, 0–2, and 0–3 bands in the PL spectrum of individual DSB HMD (Figure 2 a). This indicates the fluorescence resonance phenomenon is due to some appropriate cavity feedback, such as an FP cavity and WGM cavity. For an FP cavity, it can be formed either by the top and bottom hexagonal facets (Figure S3a) or by two opposing edge facets of the HMD (Figure S3b). Importantly, DSB HMDs could also support 6-WGM (Figure 2 d), 3-WGM (Figure 2 e), and D3-WGM (Figure 2 f), where the light is totally reflected by the six (or three) lateral sides of DSB HMDs.[19] Total internal reflection (TIR) is possible at the HMD/air or HMD/quartz interfaces only if $\phi \geq \arcsin(1/n_r)$, where ϕ is the angle of incidence light with respect to the normal of the given facet, and n_r is the relative phase refraction index. In our case, DSB HMD has two interfaces of DSB/air and DSB/quartz, where n_r equals to n_{DSB}/n_{air} and

n_{DSB}/n_{quartz}, respectively. For DSB ($n_{DSB}=2.1$), at the DSB/air interface with $n_r=2.1$ ($n_{air}=1.0$), the smallest angle of TIR is $\phi_{min,air}=28°$, and $\phi_{min,quartz}=44°$ at the HMD/quartz interface with $n_r=1.45$ ($n_{quartz}=1.45$). As shown in Figure 2d–f, $\phi=60°$ for 6-WGM and $\phi=30°$ for 3-WGM or D3-WGM are all larger than $\phi_{min,air}=28°$. Therefore, our DSB HMDs can indeed support these three WGMs. This is true even for elongated HMD microresonators (Figure S4).[19]

In a hexagonal cavity constituted by six lateral faces, 6-WGM is the most common case, and 3-WGM and D3-WGM are doubly degenerate. Figure 2c shows a μ-PL image of a single HMD, which reveals alternative bright/dark edges under laser excitation. This phenomenon is consistent with the characteristics of 3-WGM or D3-WGM microcavity, which is constituted by three lateral sides of HMD. This is in sharp contrast to ZnO HMDs, of which the μ-PL image shows six bright lateral sides due to the formation of 6-WGM.[4] Recently Zhao et al. observed the asymmetric light propagation in rhombic organic microplates of 2-acetyl-6-methylaminonaphthalene (AMN), due to the anisotropic molecular packing.[20] Spano calculated that the transition dipole moment of DSB molecule is almost parallel to the long molecular axis (Figure S5b).[14] In single-crystalline HMDs, DSB molecules adopt anisotropic herringbone packing modes. The orientation of the transition dipole moment of DSB molecules tilts at an angle of 57° with respect to HMD top/bottom surfaces bound by (001) crystal planes (Figure S5c). Upon laser excitation of HMDs, the PL light emitted by DSB molecules, which should be primarily oriented within a plane perpendicular to the transition dipole-moment, propagates obliquely upward toward the top surface and obliquely downward toward the bottom surface (Figure S5c). According to the TIR theory, the larger $n_r=2.1$ at the HMD/air interface than $n_r=1.45$ at the HMD/quartz interface results in a higher TIR efficiency and a weaker optical loss at the HMD top-face than those at the HMD bottom-face.[21] Therefore, asymmetric light propagation takes place.[20] After the obliquely upward guided PL undergoes TIR at the top-face, it could be further reflected by the given side-face (Face 1), and be coupled into 3-WGM or D3-WGM resonators selectively constituted by three facets (Face 1, Face 3, and Face 5) (see Figure S5c); however, the obliquely downward guided PL would tend to be leaked into quartz substrate.[21] That is, 3-WGM or D3-WGM could form in DSB HMD resonators, giving rise to alternative bright/dark edges. In any event, the Q factor is an important parameter to describe a laser cavity. From the experiment, the Q factor is estimated to be as high as 210 according to the definition $Q=\lambda/\Delta\lambda$, where λ is the peak wavelength (440 nm) and $\Delta\lambda$ (2.1 nm) is the line-width of the peak (Figure S6), respectively. This obtained high quality factor (Q of about 210) is reasonable for 3-WGM or D3-WGM microcavities in HMD with $d=3.0$ μm. The FP-mode cavity is absent in the HMD with such a small size of several micrometers(≈5 μm).[4] We can conclude that the observed resonance peaks could be attributed to 3-WGM or D3-WGM.

To further confirm the cavity mode, microdisks with different edge lengths were studied. μ-PL spectrum of sample HMDs are shown in Figure 2 and Figure S7. The modulation

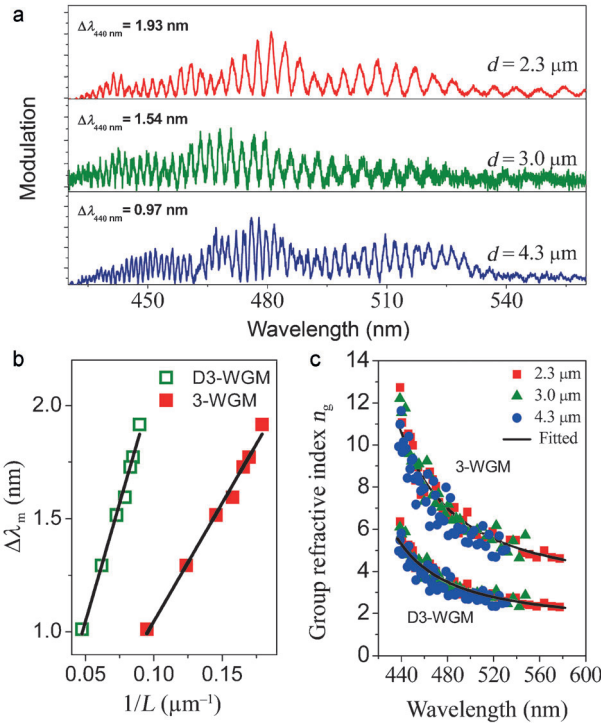

Figure 3. a) WGM modulation within the range of 430–560 nm in three HMDs with different size by removing the fluorescence background. b) The mode spacing at 440 nm (0–1) versus L^{-1} (L: the length of the round-trip in D3-WGM cavity ($4.5\times d$) and 3-WGM cavity($4.5\times d$)) of hexagonal disks, showing clearly a linear relationship. c) The plots and fitted curves of the group refractive index (based on 3-WGM and D3-WGM) versus the wavelength in three HMDs with different sizes.

of WGM resonance on the emission spectra could be better analyzed by removing the fluorescent background, as shown in Figure 3a. The spacing between two adjacent peaks ($\Delta\lambda_m$) is 1.93, 1.54, and 0.97 nm around 440 nm for three HMDs with d of 2.3, 3.0, and 4.3 μm, respectively (Figure 3a). The increasing number of modes with the increasing size of HMDs indicates that the optical modulation is certainly based on the confinement of photons within the HMD. To analyze the resonance fluorescence spectrum, the $\Delta\lambda_m$ between adjacent modes is given by the following Equation (1),

$$\Delta\lambda_m=\frac{\lambda^2}{L[n-\lambda(dn/d\lambda)]} \quad (1)$$

where n is the phase refractive index of the crystal ($n=2.1$), L is round-trip distance within a cavity mode, $dn/d\lambda$ is the dispersion relation. Figure 3b presents a plot of the mode spacing $\Delta\lambda_m$ at $\lambda=440$ nm versus 1 L ($L=4.5d$) of the 3-WGM and ($L=9.0d$) of D3-WGM, respectively, demonstrating clearly a linear relationship. This linear relationship is consistent with that the light travels in the form of 3-WGM or D3-WGM rather than other modes in the HMD resonator. According to Equation (1), the group refractive index n_g could be expressed as Equation (2).

$$n_g=n\left(1-\frac{\lambda dn}{nd\lambda}\right) \quad (2)$$

Based on the μ-PL of three individual HMDs, the n_g corresponding to the emission regime (430–560 nm) could be calculated to profile the optical dispersion relations in active cavities for 3-WGM and D3-WGM by Equation (2), as plotted in Figure 3c. The n_g (based on 3-WGM and D3-WGM) both show a curve that dramatically decreases with the increase of the wavelength at the region below 520 nm, and then reaches a stable value, which is identical in all the three HMDs with different sizes. The value of n_g (based on 3-WGM) ranges from 13.0 to 4.6, which is not consistent with previously reported n_g in organic microcrystal system.[22] Meanwhile the obtained n_g (2.3–6.5) based on D3-WGM shows a curve that dramatically decreases with the increase of wavelength at the region below 520 nm, and then reaches a stable value (ca. 2.3) close to n (2.1). It indicates that D3-WGM is reasonable for the feedback mode in the HMD microcavity. We could come to the conclusion that the assembled organic HMDs function as D3-WGM microcavity. Furthermore, these high values (ca. 6.5) of n_g at the high-energy band indicate strong exciton–photon coupling happens in this assembled HMDs and the formation of exciton–polaritons (EP) quasi-particles.[22]

Room-temperature laser oscillator could be achieved in individual HMD by increasing the pump density of optical excitation. The dependence of photoluminescence spectrum on the pump density (obtained from one HMD with $d =$ 2.7 μm) is shown in Figure 4a. When the pump density exceeds a threshold from $P = 820$ to 1170 nJ cm^{-2}, strong laser emission emerges as a set of sharp peaks on the top of the 0–1 transition. It is consistent with that 0–1 transition has the maximum net gain in four-level organic laser system.[15] The mode spacing $\Delta\lambda_m$ is the same below and above the threshold. This demonstrates that the lasing actions are from the D3-WGM feedback resonators. Above the threshold of lasing, the brighter dots (Figure 4b) on alternative bright edges of HMD appear. This indicates these three corresponding faces constitute the feedback cavity, which is indispensable for lasing oscillation. Figure 4c shows the integrated intensities of the 0–1 peak as a function of pump density, demonstrating a threshold at $P_{th} = 790$ nJ cm^{-2}. The intensity dependence is fitted to power law x^p and $p = 0.46 \pm 0.02$ below threshold, assigned to a sublinear regime where bimolecular quenching (exciton–exciton annihilation) dominates,[23] and $p = 2.59 \pm 0.02$ above the threshold ascribed to superlinear regime are achieved. In sharp contrast, the 0–2 band remains in the sublinear regime ($p = 0.47 \pm 0.02$) both below and above threshold.

To further verify the lasing action, we investigated the PL lifetimes with a streak camera (Figure 4d). The individual HMD PL follows single exponential decay with $\tau = 1.81 \pm 0.04$ ns at a very low excitation density of $0.04\,P_{th}$. Upon increasing the pump intensity to $P = 0.15\,P_{th}$ and $0.71\,P_{th}$, bi-exponetial PL decay takes place with the short component ascribed to the presence of bimolecular quenching.[23] Above the threshold, for example, at $1.83\,P_{th}$, the PL decay time always collapses to < 10 ps and is limited by the resolution of our apparatus. This short PL lifetime above the threshold suggests the process of lasing action occurs in the HMD.

As compared with multi-mode lasing, single-mode lasing has its inherent merits as good stability of laser oscillation due to the absent of mode-competition, excellent monochrome properties of laser beam, and fine optical coherence. In principle, the gain of lasing action is determined by the spatial spectra and the spectral overlap between the resonance and the gain material.[24] The absorption and fluorescence emission of DSB HMDs are plotted in the inset of Figure 5, where the patterned area represents the region where the net optical gain can be achieved. Given that smaller resonators contain

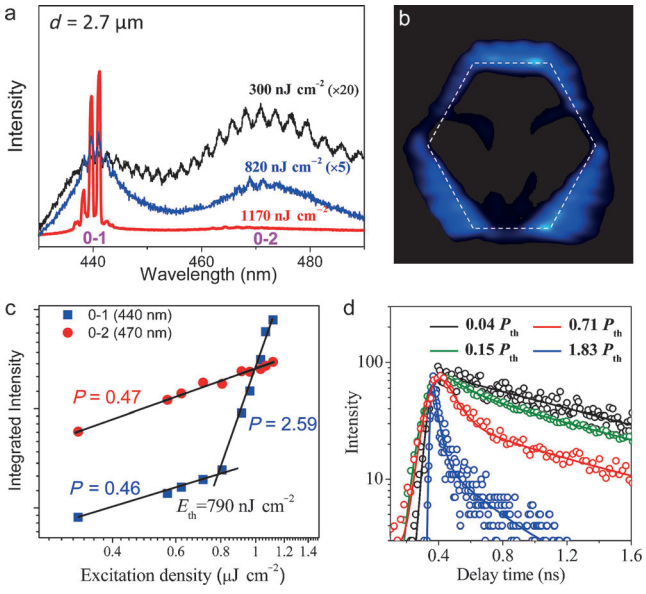

Figure 4. a) The μ-PL spectra of the individual HMD with the edge length 2.7 μm under different pump pulse energies at room temperature. b) PL image of the corresponding disk above the threshold. c) Integrated area of the 0–1 peak and 0–2 peak as a function of pump density. The lasing threshold is identified as the intersection between the sublinear and superlinear regions. d) PL decay profiles of the same HMD excited at different energies.

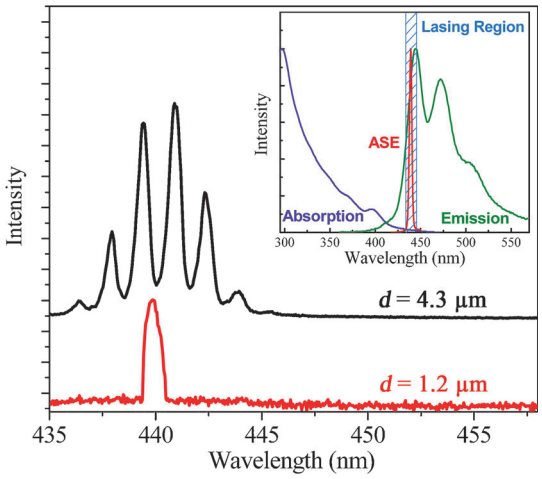

Figure 5. Single-mode lasing spectrum of a HMD with $d = 1.2$ μm and multimode lasing spectrum of a HMD with $d = 4.3$ μm. Inset: Absorption and emission of spectra of DSB single crystals, amplified spontaneous emission (ASE) of single crystals, and the patterned area presents the optical gain region of DSB.

less resonance peaks, single mode lasing could be achieved. If the mode spacing ($\Delta\lambda_m = 5$ nm) from the WGM cavity is comparable to the half of the peak width (10 nm) of the lasing region, single mode lasing could be obtained.[24] According to Equation 1, the $\Delta\lambda_m = 5$ nm can be achieved in HMD with edge length around 1.0 μm. In the experiment, we have indeed observe single mode lasing in small HMD with $d =$ 1.2 μm (Figure 5). In contrast, multiple modes are observed from a HMD with $d = 4.3$ μm.

In summary, we have demonstrated WGM resonator on self-assembled organic DSB hexagonal microdisks (HMDs) with the edge length (d) ranging from 1.0–5.0 μm. Pumped by laser, photoluminescence (PL) microscopy reveals alternative bright/dark edges on DSB HMDs characteristic of D3-WGM resonator. Its corresponding emission spectrum shows room temperature resonance phenomena. And optically pumped lasing was observed in these organic HMDs above a threshold of 790 nJ cm^{-2}. More importantly, single mode lasing can be achieved in smaller HMD ($d = 1.2$ μm). These easily fabricated organic single-crystalline microdisks at the microscale can act as the laser source, which offer potential applications as adaptable photonic components.

Received: December 9, 2013
Revised: February 17, 2014
Published online: April 24, 2014

Keywords: microdisk laser · nanophotonics · organic nanostructures · self-assembly · whispering-gallery mode

[1] S. L. McCall, A. F. J. Levi, R. E. Slusher, S. J. Pearton, R. A. Logan, *Appl. Phys. Lett.* **1992**, *60*, 289.
[2] K. Srinivasan, O. Painter, *Nature* **2007**, *450*, 862.
[3] L. He, S. K. Özdemir, L. Yang, *Laser Photonics Rev.* **2013**, *7*, 60.
[4] R. Chen, B. Ling, X. W. Sun, H. D. Sun, *Adv. Mater.* **2011**, *23*, 2199.
[5] A. C. Tamboli, E. D. Haberer, R. Sharma, K. H. Lee, S. Nakamura, E. L. Hu, *Nature* **2007**, *445*, 61.
[6] R. Chen, T. D. Tran, K. W. Ng, W. S. Ko, L. C. Chuang, F. G. Sedgwick, C. C. Hasnain, *Nat. Photonics* **2011**, *5*, 170.
[7] E. D. Haberer, R. Sharma, C. Meier, A. R. Stonas, S. Nakamura, S. P. DenBaars, E. L. Hu, *Appl. Phys. Lett.* **2004**, *85*, 5179.
[8] C. Kim, Y. J. Kim, E. S. Jang, G. C. Yi, H. H. Kim, *Appl. Phys. Lett.* **2006**, *88*, 093104.
[9] J. Clark, G. Lanzani, *Nat. Photonics* **2010**, *4*, 438.
[10] S. V. Frolov, Z. V. Vardeny, K. Yoshino, *Appl. Phys. Lett.* **1998**, *72*, 1802.
[11] H. Taniguchi, T. Fujiwara, H. Yamada, S. Tanosaki, M. Baba, *Appl. Phys. Lett.* **1993**, *62*, 2155.
[12] C. Zhang, C. L. Zou, Y. Yan, R. Hao, F. W. Sun, Z. F. Han, Y. S. Zhao, J. N. Yao, *J. Am. Chem. Soc.* **2011**, *133*, 7276.
[13] L. T. Kang, H. B. Fu, X. Q. Cao, Q. Shi, J. N. Yao, *J. Am. Chem. Soc.* **2011**, *133*, 1895.
[14] F. C. Spano, *J. Chem. Phys.* **2003**, *118*, 981.
[15] I. D. W. Samuel, G. A. Turnbull, *Chem. Rev.* **2007**, *107*, 1272.
[16] C. C. Wu, O. J. Korovyanko, M. C. Delong, Z. V. Vardeny, J. P. Ferraris, *Synth. Met.* **2003**, *139*, 735.
[17] Z. Z. Xu, Q. Liao, Q. Shi, H. L. Zhang, J. N. Yao, H. B. Fu, *Adv. Mater.* **2012**, *24*, OP216.
[18] F. C. Spano, *Acc. Chem. Res.* **2010**, *43*, 429.
[19] M. Grundmann, C. P. Dietrich, *Phys. Status Solidi B* **2012**, *249*, 871.
[20] W. Yao, Y. L. Yan, L. Xue, C. Zhang, G. P. Li, Q. D. Zheng, Y. S. Zhao, H. Jiang, J. N. Yao, *Angew. Chem.* **2013**, *125*, 8875; *Angew. Chem. Int. Ed.* **2013**, *52*, 8713.
[21] G. Zhu, C. X. Xu, L. S. Cai, J. T. Li, Z. L. Shi, Y. Lin, G. F. Chen, T. Ding, Z. S. Tian, J. Dai, *ACS Appl. Mater. Interfaces* **2012**, *4*, 6195.
[22] K. Takazawa, J. Inoue, K. Mitsuishi, T. Takamasu, *Phys. Rev. Lett.* **2010**, *105*, 067401.
[23] S. Kéna-Cohen, S. R. Forrest, *Nat. Photonics* **2010**, *4*, 371.
[24] R. Chen, T. Van Duong, H. D. Sun, *Sci. Rep.* **2012**, *2*, 244.

